

**Effect of sample heterogeneity on the interpretation of QCM(-D) data:  
Comparison of combined QCM/AFM measurements with  
finite element method (FEM) modeling**

Diethelm Johannsmann,<sup>1\*</sup> Ilya Reviakine,<sup>2\*</sup> Elena Rojas,<sup>2</sup> Marta Gallego<sup>2</sup>

<sup>1</sup>Institute of Physical Chemistry, Clausthal University of Technology, Clausthal-Zellerfeld, D-38678, Germany.

<sup>2</sup>Centro de Investigacion Cooperativa en Biomateriales, Parque Tecnológico de San Sebastián, E-20009 San Sebastián, Spain.

### **Supporting Information**

Below we provide details of the simulation. We used the Multiphysics Module of the COMSOL software package (COMSOL GmbH, Göttingen, Germany). Within the FEM approach, one models the adsorbate as a continuous medium with given density and viscoelastic constants. The adsorbed protein does not have internal structure.

The computational resources available to us only allowed for two-dimensional simulations. In principle, 3D calculations are possible with the COMSOL Multiphysics package. However, the results depended on the details of the meshing at all mesh sizes which we could afford. Because of the 2D nature of the simulation, the geometry corresponds to adsorbed cylinders, rather than spheres. The cylinders may either be oriented perpendicular (Fig. 4a-c) or parallel (Fig. 4d) to the direction of flow. We did not study inclined orientations. When comparing experimental results and modeling results, we use arithmetic averages calculated for perpendicular and for parallel direction of flow.

A further simplification concerns periodicity. We applied periodic boundary conditions at the top and bottom in Figs. 3 and 4. The periodicity *is* of some influence. We checked by enlarging the cell and placing more than one cylinder into the enlarged cell. This geometry

---

\*Authors for correspondence: [johannsmann@pc.tu-clausthal.de](mailto:johannsmann@pc.tu-clausthal.de), [ireviakine@cicbiomagune.es](mailto:ireviakine@cicbiomagune.es).

was still periodic, but the unit cell was larger and contained a pseudo-random arrangement of spheres. Varying the locations of the spheres did affect the results. In terms of numerical accuracy, such large cells again challenge the computing power of a normal PC and therefore entail compromises with regard to the resolution of the mesh. For this reason, we base the analysis on a strictly periodic geometry.

With regard to the shape of the adsorbed molecule, we tested two geometries, which were a truncated cylinder (Fig. 3a) and a hemicylinder (Fig 3b). In the first case, the sphere diameter was 12 nm, and the compression at the surface was 1 nm. In the second case, the diameter was 15.2 nm. This value was chosen such that the volume of the two is the same (in 3D). For cylinders aligned perpendicular to the direction of shear, we employed the 2D steady-state incompressible Navier-Stokes model (Fig. 4a–c). Along the surface normal, the cell was 2  $\mu\text{m}$  long, which amounts to 8 times the penetration depth of the acoustic shear wave at 5 MHz. The penetration depth,  $\delta$ , is 252 nm on the fundamental. Neutral boundary conditions were applied at the domain boundaries on the right, the top, and at the bottom. The left hand side oscillated with an amplitude of  $u_0 = 10^{-2}$  nm. More technically, the boundary was assigned a fixed “velocity”, where the velocity was defined as  $i\omega u_0$ . With regard to the mesh size, the default settings were modified in one respect, which was the maximum mesh size at the three-phase line (or, in 2D, the three-phase point) between the water, the adsorbate, and the wall. This was set to 0.001 nm.

The steady-state incompressible Navier-Stokes model of the COMSOL Multiphysics package is geared to steady (rather than oscillatory) movement. However, all variables (including speed and pressure) can be made complex. The model readily produces oscillating shear waves if the term  $-i\omega\rho v$  ( $\rho$  the density and  $v$  the local speed) is inserted for the body force in the subdomain settings. COMSOL always plots the real parts of speed and pressure (Fig. 4) when outputting the solution. In order to visualize the imaginary part, one uses an

imaginary speed of motion at the left-hand domain boundary (thereby multiplying the entire solution with a factor of  $i$ ).

Fig. 9 in the main text shows the tangential stress at the crystal surface. Typical for contacts between mechanically dissimilar materials, there is a sharp peak of stress close to the three-phase line. The integrated tangential force onto the left-hand side of the cell was calculated in the Post Processing Mode. Division by the height of the cell yields the stress,  $\sigma$ . This stress is inserted into the small-load approximation <sup>1,2</sup>

$$\frac{\Delta f^*}{f_F} \approx \frac{i Z_L}{\pi Z_q} = \frac{i \sigma}{\pi Z_q \dot{u}} \quad \text{Eq. 1}$$

which then leads to  $\Delta f$  and  $\Delta \Gamma$ . The values displayed in Figs. 2, 5, 6, and 7 of the main text are differences in  $\Delta f$  and  $\Delta \Gamma$  between a crystal loaded with a liquid and a particle, on the one hand, and a crystal loaded with the liquid only, on the other. The latter situation produces a frequency shift of -716 Hz (relative to the bare crystal in the absence of liquid). Given that the data shown in Figs. 2, 5, 6, and 7 are differences of large numbers, the requirements with regard to accuracy of the simulations are quite severe.

The water phase was assumed to have a density of  $1 \text{ g/cm}^3$  and a viscosity of  $\eta = 1 \text{ mPa s}$ . The particle was assumed to have a viscosity of  $\eta^* = (\eta'^2 + \eta''^2)^{1/2} = 100 \text{ Pa s}$ . The particle is viscoelastic ( $\eta = \eta' - i\eta''$ ), where the loss tangent ( $\tan \delta_L = \eta''/\eta'$ ) was chosen as 0.16. The exact value of the particle's modulus does not matter as long as the particle is much stiffer than the liquid. As discussed in the results section of the main text, effects of finite stiffness are stronger for adsorbed spheres than for planar films. The modeling of particles with a stiffness comparable to the stiffness of water (such as vesicles) is outside the scope of this work, although it certainly deserves attention.

For the simulation of shear flow *along* the cylinder direction, we used the COMSOL's steady-state diffusion model. The speed in this case only has a single non-trivial component, directed perpendicular to the plane of the paper in Fig. 4d. The speed (or, more precisely, the momentum) obeys a diffusion equation, where the role of the diffusivity is taken by the kinematic viscosity,  $\eta/\rho$ . In order to recover oscillating shear waves, the term  $-i\omega c$  ( $c$  the “concentration”, equivalent to momentum) must be inserted for the reaction rate in the subdomain settings.

We checked for a dependence of  $\Delta f$  and  $\Delta\Gamma$  on oscillation amplitude and found it to be completely insignificant (fractional changes in  $\Delta f$  and  $\Delta\Gamma$  below the numerical reproducibility) at amplitudes below 1 nm (Fig. S1). This is consistent with the recent experimental work on the effect of oscillation amplitude on the QCM response from the adsorbing polymer microspheres.<sup>3</sup> There are two mechanisms, by which a high oscillation amplitude might influence the results. Firstly, the nonlinear term in the Navier-Stokes equation ( $\rho(\mathbf{v}\cdot\nabla)\mathbf{v}$ , with  $\rho$  the density and  $\mathbf{v}$  the speed) will produce a Bernoulli pressure. Secondly, the simulation at this point does not employ a deformable mesh. More technically, we use Lagrangian coordinates, as opposed to Euler coordinates. As a consequence, the domain boundaries do not adapt to the flow. At small amplitudes, this artifact is irrelevant because the shear angle,  $\gamma$ , is small. The shear angle is of the order of the amplitude of oscillation ( $10^{-2}$  nm) divided by the penetration depth ( $\sim 100$  nm, depending on overtone order). At high amplitudes ( $> 10$  nm, see Fig. S1), the artifact is noticeable. The above remarks evidently only concern the FEM calculation. In experiment, other effects (like a detachment of the spheres from the surface<sup>Error! Bookmark not defined.</sup>) might come into play.

In the absence of adsorbed particles, the simulation reproduces the Gordon-Kanazawa result ( $\Delta f = -f_F(\rho\omega\eta/2)^{1/2}/(\pi Z_q)$ , with  $\rho$  the density and  $\eta$  the viscosity) within 0.1 %. For homogenous films, the Sauerbrey equation ( $\Delta f = -f_F\omega m_f/(\pi Z_q)$  with  $m_f$  the areal mass density

of the film) is reproduced to within 0.1%. The film resonance (eq. 7 in Ref. 4) is reproduced within 1% (Fig. S2).

A more challenging test concerns shallow surface corrugation gratings as treated by Urbakh and Daikhin.<sup>5</sup> These predictions are reproduced to within 0.5 Hz. Fig. S3 shows the geometry and the solution of the flow profile. A rigid sheet ( $G = 3$  GPa) with an average thickness of 21 nm was placed onto the resonator surface. The interface between this layer and the liquid was corrugated, where the sinusoidal corrugation assumed in Ref. 5 was approximated by a third order Bezier line. The shifts of frequency and bandwidth were referenced to the same sheet with no corrugation. Fig. S4 shows  $\Delta f$  and  $\Delta\Gamma$  versus amplitude of corrugation. The dashed line is the analytical result for the frequency shift on the fundamental, which is

$$\begin{aligned}\frac{\Delta f}{f_F} &= -\frac{1}{\pi Z_q} \sqrt{\frac{\omega \rho \eta}{2}} \left(\frac{h}{\delta}\right)^2 \bar{q} F \\ \frac{\Delta \Gamma}{f_F} &= \frac{1}{\pi Z_q} \sqrt{\frac{\omega \rho \eta}{2}} \left(\frac{h}{\delta}\right)^2 \bar{q} G \\ F &= \sqrt{\sqrt{1+2\bar{q}^{-4}} + 1} - \sqrt{2\bar{q}^{-1}} + \sqrt{2} \cos^2 \varphi \\ G &= -\sqrt{\sqrt{1+2\bar{q}^{-4}} - 1} + \sqrt{2\bar{q}^{-1}} \\ \bar{q} &= \frac{2\pi\delta}{L}\end{aligned}\tag{Eq. 2}$$

Here  $h$  is the amplitude of corrugation and  $L$  is its periodicity.  $\varphi$  is the angle between the direction of corrugation and the direction of flow. We used  $\varphi = 0$ , which implies a flow perpendicular to the grooves. In the limit of small-amplitude corrugation,  $\Delta f$  is as parabolic function of  $h$ . The overtone dependence is so weak that it would be hardly distinguishable in the plot.  $\Delta\Gamma$  is below 0.04 Hz, in accordance with the analytic result.

In the following we show that the artifacts introduced by a stationary mesh vanish in the small amplitude limit. The COMSOL code in its most simple version does not adapt the

mesh to the flow. As a consequence, the domain boundaries remain immobile, which clearly is unphysical for deformable objects.

Let the solution to the problem with fixed boundaries be called  $(u, p)$  with  $u$  the velocity field and  $p$  the pressure. Let the solution of the problem with moving boundaries be called  $(u + \delta u, p + \delta p)$ . Let the scalar field of viscosity be called  $\eta$  for fixed boundaries and  $\eta + \delta\eta$  for the moving boundaries.  $\delta\eta$  only is nonzero close to the boundaries, where – depending on whether boundaries move or not – the viscosity at this specific locations may change upon particle deformation. We employ Euler coordinates, which do not move with the medium.  $\delta\eta$  is *not* small.  $\delta u$  and  $\delta p$ , on the other hand, *are* small, as we show below.

$u$  and  $p$  are the solution to the partial differential equation

$$\begin{aligned} \rho \frac{\partial u}{\partial t} + \rho(u \cdot \nabla)u + \nabla \cdot (\eta \nabla u) - \nabla p = & \\ i\omega \rho u + \rho(u \cdot \nabla)u + \nabla \eta \cdot \nabla u + \eta \nabla^2 u - \nabla p = 0 & \end{aligned} \quad \text{Eq. 3}$$

Note that the gradients may be sharp at the boundaries. We assume that the boundaries have a finite (albeit small) width, such that all derivatives remain well-defined. Now let the boundary itself undergo an oscillatory movement. The scalar field of the viscosity,  $\eta(r)$  then turns into the modified field  $(\eta + \delta\eta)(r, t)$ , where the difference is nonzero only in those regions, which are covered by the movement of the boundary. In response to the shift in viscosity, the vector field  $u(r)$  and the pressure field  $p(r)$  turn into modified fields  $(u + \delta u)(r)$  and  $(p + \delta p)(r)$ . There is second change in the differential equation, which concerns the time derivative of speed. Since the boundary now moves with the fluid, the nonlinear term  $u \cdot \nabla u$  vanishes. There is no artificial acceleration due to particles crossing a boundary. (We work at low Reynolds numbers, where the nonlinear term in the bulk is negligible. The nonlinear term only matters, if material crosses a boundary.) The modified differential equation therefore reads.

$$\begin{aligned} i\omega\rho(u + \delta u) + \nabla(\eta + \delta\eta) \cdot \nabla(u + \delta u) \\ + (\eta + \delta\eta)\nabla^2(u + \delta u) - \nabla(p + \delta p) = 0 \end{aligned} \quad \text{Eq. 4}$$

Subtracting Eq. 3 from Eq. 4 yields

$$\begin{aligned} i\omega\rho\delta u + (\eta + \delta\eta)\delta\eta\nabla^2\delta u + \nabla(\eta + \delta\eta) \cdot \nabla\delta u - \nabla\delta p \\ = -\delta\eta\nabla^2u - \nabla\delta\eta \cdot \nabla u = S \end{aligned} \quad \text{Eq. 5}$$

This is an inhomogeneous partial differential equation in  $(\delta u, \delta p)$ . The term on the right-hand side is a source term, abbreviated  $S$ . The solution to Eq. 5 typically is calculated by means of the Greens formalism. One calculates a three-component Greens function  $G = (G_{ux}, G_{uy}, G_p)$  obeying

$$\begin{aligned} i\omega\rho G(r - r') + (\eta + \delta\eta)\nabla^2 G(r - r') \\ + \nabla(\eta + \delta\eta) \cdot \nabla G(r - r') - \nabla G(r - r') = \delta(r - r') \end{aligned} \quad \text{Eq. 6}$$

The Greens function is related to the Oseen tensor. For the following argument, it is not necessary to actually calculate  $G$ . One can see that the changes in the fields  $\delta u$  and  $\delta p$  vanish in the small-amplitude limit without explicitly writing them down. It suffices to realize that  $G$  exists and is unique. Once  $G$  has been found, one can – in principle – calculate the solution  $(\delta u_x, \delta u_y, p)$  by an integration over the source term

$$\begin{pmatrix} \delta u_x(r) \\ \delta u_y(r) \\ \delta p(r) \end{pmatrix} = \int_{Volume} G(r - r') S(r') d^2 r' \quad \text{Eq. 7}$$

Importantly, the source term is only nonzero in those regions, which are covered by the moving boundaries. The volume of this region scales with the amplitude of oscillation,  $u_0$ . The integrand contains the vector field  $u(r)$ , and therefore also scales with amplitude. The source term therefore scales as  $u_0^2$  (area of integration times value of integrand) and so does the solution on the left-hand side.

The viscous stress at the interface is given by

$$\sigma_{xz} = \eta \frac{\partial(u_x + \delta u_x)}{\partial z} \quad \text{Eq. 8}$$

In the small-amplitude limit, the second term is negligible compared to the first. It scales as  $u_0^2$ , whereas the first scales as  $u_0$ . The correction induced by the moving boundaries may therefore be ignored.

## References

- 1 Eggers, F.; Funck, Th., *J. Phys. E: Sci. Instrum.* **1987**, 20, 523.
- 2 Johannsmann, D.; Mathauer, K.; Wegner, G.; Knoll, W., *Phys. Rev. B* **1992**, 46, 7808.
- 3 Edvardsson, M.; Rodahl, M.; Kasemo, B.; Hook, F. *Anal. Chem.* **2005**, 77, 4918.
- 4 Domack, A.; Prucker, O.; Rühle, J.; Johannsmann, D., *Phys. Rev. E* **1997**, 56, 680.
- 5 Urbakh, M.; Daikhin L., *Physical Review B* **1994**, 49, 4866.

## Figure Captions

**Fig. S1:** Dependence of  $\Delta f$  and  $\Delta\Gamma$  on oscillation amplitude for a truncated sphere. The coverage was 60%, the density was  $1.6 \text{ g/cm}^3$ . The default setting for the amplitude was  $10^{-2} \text{ nm}$ . The direction of flow was perpendicular to the direction of the cylinders.

**Fig. S2:**  $\Delta f$  and  $\Delta\Gamma$  versus film thickness for a film with a viscosity of  $9.87 - i 1.56 \text{ mPa s}$ . The data for the 13<sup>th</sup> overtone is presented. Film resonance (Ref. 4) is clearly reproduced.

**Fig. S3:** Geometry underlying the test of the analytical result from Ref. 5 for shallow sinusoidal waves. a): Vertical component of flow field. b): Horizontal component of flow field c): Pressure. The solid film with a corrugated surface had an average thickness of 21 nm and a stiffness of 3 GPa.

**Fig. S4:** Shifts of frequency and bandwidth for a surface with sinusoidal corrugation as shown in Fig. S3. The x-axis is the vertical amplitude of the corrugation. The wavelength is 20 nm, and the direction of flow is perpendicular to the grooves. The dashed line is the analytical result from Ref. 5.

Fig. S1

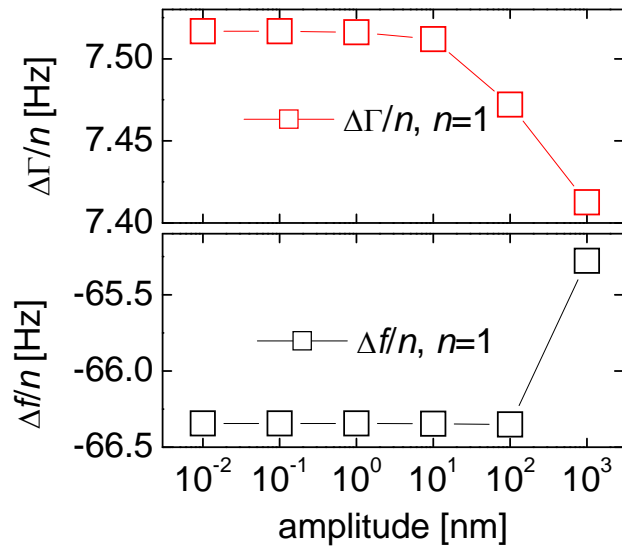


Fig. S2

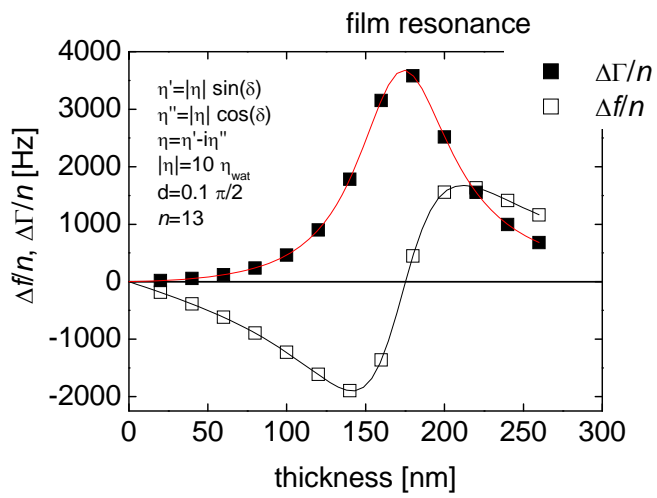


Fig. S3

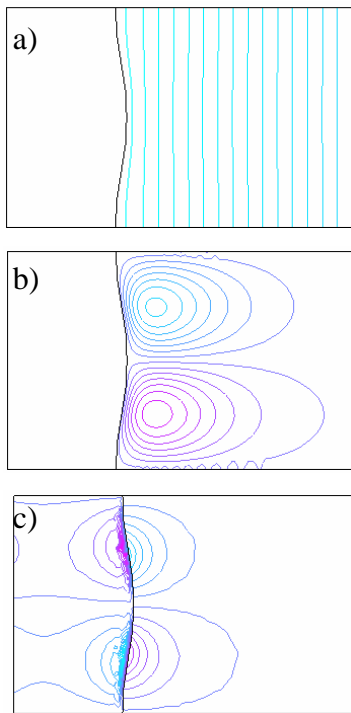


Fig. S4

